Electrokinetics of the Silica-Solution Interface: A Flat Plate Streaming Potential Study

Peter J. Scales,* Franz Grieser, and Thomas W. Healy

School of Chemistry, University of Melbourne, Parkville, Victoria 3052, Australia

Lee R. White and Derek Y. C. Chan

Department of Mathematics, University of Melbourne, Parkville, Victoria 3052, Australia

Received October 9, 1990. In Final Form: December 5, 1991

Details for the construction of a flat plate streaming potential apparatus are presented. Measurements using this apparatus on fused silica slides are reported and analyzed on the basis of a Gouy-Chapman-Stern-Grahame (GCSG) model for the electrical double layer at the silica-aqueous solution interface. It is found that the GCSG model can only partly account for the experimental results. Possible reasons for the discrepancy between experiment and theory are discussed.

Introduction

Applying a pressure gradient to a conducting fluid across a capillary or porous plug of dielectric material gives rise to a streaming potential between the capillary ends. This streaming potential that can be generated at a solid-liquid surface is a particularly useful electrokinetic measurement for characterizing the electrical double layer properties of metal oxide-aqueous solution interfaces. Apparatus using a variety of capillary configurations have been reported in the literature. These include circular capillaries,[1-3] packed plugs of particles,[4,5] parallel circular disks,[6,7] and parallel flat plates.[8,9] The design of each apparatus is centered around the fiber, particulate, or sheetlike nature of the solid under investigation. It has also been demonstrated that apparatus incorporating parallel plates or disks are well suited for studying the electrokinetics of metal oxides, synthetic sapphire, muscovite mica, glass, polymer, and coated glass surfaces.[6-9] Other workers, such as Wiese et al.[1] have used circular capillaries to study metal ion binding to fused silica. Bijsterbosch et al.[5] have used a porous plug apparatus to study polystyrene lattices.

Our interest in extending our study of Langmuir-Blodgett and other adsorbed molecular layers on silica surfaces required the choice of a flat plate or disk apparatus. The design of the flat plate streaming potential apparatus proposed by Van Wagenen and Andrade[8] appeared the most appropriate. Their apparatus uses a capillary formed between two microscope slides of dimensions 7.6 × 2.5 × 0.1 cm^3 with a Teflon or Silastic spacer gasket. The major design advantages of this type of arrangement are the simplified hydrodynamics involved and the ability to investigate simultaneously other bulk and surface properties by ellipsometry, internal reflectance spectroscopy, light and electron microscopy, and wetting techniques.

This paper examines the charge generation process at the SiO_2-solution interface and the structure of the interface. This is preceeded by a detailed description of the flat plate streaming potential apparatus used in the study. Electrokinetic data for silica are presented and the ability of the Gouy-Chapman-Stern-Grahame (GCSG) model of the electrical double layer (edl) in describing the charge-potential relationship of this oxide surface is critically examined.

Experimental Section

Apparatus. In designing and developing a flat plate streaming potential apparatus, one must consider the physical and hydrodynamic constraints that control flow in a charged capillary. Smoluchowski[10] demonstrated that for the case of an applied pressure gradient across a charged capillary, the zeta potential (ζ) is given by

$$\zeta = \left(\frac{\eta\lambda}{D\epsilon_0}\right)\left(\frac{\Delta E}{\Delta P}\right) \quad (1)$$

where λ is the conductivity of the capillary, ϵ_0 is the permittivity of free space, η is the viscosity of the fluid, ΔE is the streaming potential, and ΔP is the applied pressure gradient across the capillary.

The development of eq 1 follows from the well-known Navier-Stokes equation under steady-state conditions. The equation assumes a laminar and established flow profile in the capillary, and for any new instrument one is obliged to test that these criteria are being maintained under the proposed experimental conditions.

With this in mind, we can develop the appropriate hydrodynamic equations and calculate the average fluid velocity (v) and flow rate (Q). For a rectangular capillary of length l in the y-direction, width w in the x-direction, and height h in the z-direction, it can be shown (Appendix) that the fluid velocity

* Author to whom correspondence should be addressed.

(1) Wiese, G. R.; James, R. O.; Healy, T. W. *Discuss. Faraday Soc.* **1972**, *52*, 302.

(2) Van Wagenen, R. A.; Andrade, J. D.; Hibbs, J. B. *J. Electrochem. Soc.* **1976**, *123*, 1438.

(3) Grieser, F.; Lamb, R. N.; Wiese, G. R.; Yates, D. E.; Cooper, R.; Healy, T. W. *Radiat. Phys. Chem.* **1984**, *23*, 43.

(4) Li, H. C.; De Bruyn, P. L. *Surf. Sci.* **1966**, *5*, 203.

(5) Hidalgo-Alvarez, R.; De Las Nieves, F. J.; Van der Linde, A. J.; Bijsterbosch, B. H. *Colloids Surf.* **1986**, *21*, 259.

(6) Lyons, J. S.; Furlong, D. N.; Homola, A.; Healy, T. W. *Aust. J. Chem.* **1981**, *34*, 1167.

(7) Street, N. *Aust. J. Chem.* **1964**, *17*, 828.

(8) Van Wagenen, R. A.; Andrade, J. D. *J. Colloid. Interface Sci.* **1980**, *76*, 305.

(9) Bousse, L.; Mostarshed, S.; Van Der Shoot, B.; De Rooij, N. F.; Grimmel, P.; Göpel, W. *J. Colloid Interface Sci.* **1991**, *147*, 22.

(10) Hunter, R. J. *Zeta potential in colloid science*; Academic Press: London, 1981; p 66.

0743-7463/92/2408-0965$03.00/0

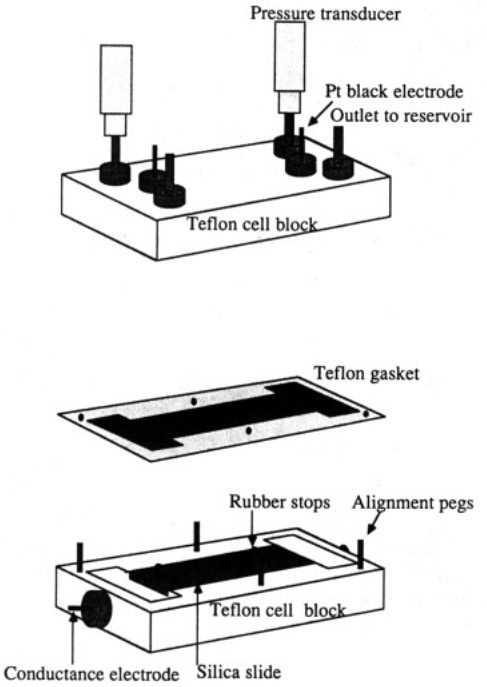

Figure 1. Schematic diagram of the cell used for streaming potential measurements.

profile in the y-direction through the capillary is given by

$$v(x,z) = \left(\frac{z(h-z)\Delta P}{2\eta l}\right) - \left(\frac{4h^2\Delta P}{\pi^3 l\eta}\right)\sum_{m=0}^{\infty}\left[\left(\frac{1}{(2m+1)^3}\right)\left(\frac{\cosh\left(\frac{(2m+1)\pi}{h}\left(x-\frac{w}{2}\right)\right)}{\cosh\left(\frac{(2m+1)\pi w}{2h}\right)}\right)\sin\left(\frac{(2m+1)\pi z}{h}\right)\right] \quad (2)$$

and the flow rate by

$$Q = \int_0^w dx \int_0^h dz\, v(x,z)$$

$$= \left(\frac{wh^3\Delta P}{12\eta l}\right) + \left(\frac{16h^4\Delta P}{\pi^5\eta l}\right)\sum_{m=0}^{\infty}\left(\frac{\tanh\left(\frac{(2m+1)\pi w}{2h}\right)}{(2m+1)^5}\right) \quad (3)$$

The testing of these flow equations is obligatory to a full understanding of the limits of the streaming potential technique in the format proposed. The apparatus used is shown in Figures 1 and 2. The streaming potential cell was constructed from two Teflon blocks each with an accurately cut depression to take a streaming potential plate of dimensions $2.5 \times 7.5 \times 0.1$ cm^3. Each plate was held firmly in position by two Viton rubber stops. A small reservoir was machined into each end of the base block. The Teflon blocks were separated by a Teflon gasket of 0.0120 cm thickness and aligned with four stainless steel pegs. A capillary of dimensions $2.20 \times 7.50 \times 0.0120$ cm^3 was formed between the two plates by clamping the cell together with a perspex clamp. The pressure drop (ΔP) across the ends of the capillary was monitored with two Kulite Model IPT-1100-10SG solid-state pressure transducers. Transducer output was subtracted using operational amplifiers and calibrated using a mercury manometer over a wide pressure range. The differential pressure was recorded on one channel of a Curken twin-pen chart recorder. ΔP across the capillary was then calculated using the predetermined calibration factor and was precise to ± 10 N m^{-2}.

The streaming potential (ΔE) across the capillary was measured by connecting an Analogue Devices Model 515 JH electrometer

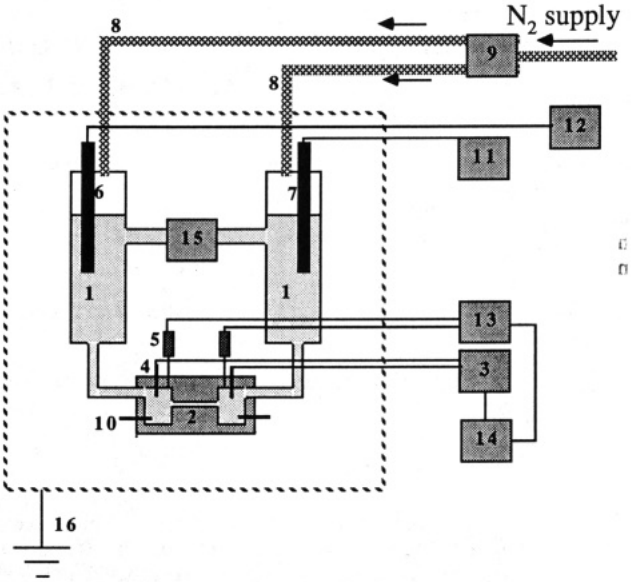

Figure 2. Overview of the apparatus used for streaming potential measurements: (1) electrolyte reservoirs; (2) streaming potential cell; (3) high impedance chip; (4) streaming potential electrodes; (5) pressure transducer; (6) pH electrode; (7) conductivity probe; (8) gas line; (9) two-way solenoid valve; (10) conductance electrodes; (11) conductivity meter; (12) pH meter; (13) transducer power supply; (14) dual pen chart recorder; (15) peristaltic pump; (16) Faraday cage.

chip with an input impedance of $>1 \times 10^{14}$ Ω across the measuring electrodes. The output from the chip was recorded on the opposing channel of a Curken chart recorder. Electrodes were platinized platinum and were renewed regularly. The electrodes were positioned in the upper Teflon block of the streaming potential cell. Another set of electrodes for conductance measurements were positioned in the lower Teflon block. Dependent upon the mode of measurement, these electrodes were either reversible Ag/AgCl or platinized platinum.

The streaming potential cell was connected via a wide bore silica tube to two 500 cm^3 electrolyte reservoirs. The pH of the electrolyte was measured using a Titron combined low leak pH electrode and Radiometer Model pHm84 research pH meter. The bulk conductivity was measured using a Titron conductivity probe and a Philips Model PW 9526 digital conductivity meter. The conductivity probe was calibrated with Stokes solutions[11] prepared with ultrapure potassium chloride (>99.99%, Fluka).

Nitrogen gas was used to create the ΔP across the capillary. A twin Martonair solenoid system was used to direct gas pressure to one reservoir while exposing the other to atmosphere. Electrolyte was circulated between measurements with a peristaltic pump located between the electrolyte reservoirs and connected with high-grade silastic tubing. All other connections and connectors were made of wide bore Teflon or glass.

The streaming potential cell, electrolyte reservoirs, and peristaltic pump were enclosed in an earthed Faraday cage.

Potential–Pressure Curves. The zeta potential, ζ, at the shear plane of a solid, was related to measured values of ΔE and ΔP using eq 1. Literature values of η and D and bulk values of λ were used. ΔE and ΔP were output directly to a twin-pen chart recorder from the streaming potential cell. ΔE was then plotted against ΔP after subtracting out asymmetry potentials associated with the finite surface area and nonreversibility of the measuring electrodes.

Ten pairs of values of ΔP against ΔE were recorded for each measurement of ζ with liquid being displaced in both directions in the capillary. A linear least-squares assessment was made of each data set and the slope of the line used to evaluate ζ. Good linearity was observed in both flow directions. Plots showing poor linearity or with asymmetry potentials in excess of ±30 mV were rejected. Asymmetry potentials were reduced by keeping

(11) Robinson, R. A.; Stokes, R. H. *Electrolyte Solutions*, 2nd ed.; Butterworths Scientific Publishers: London, 1959; p 158.

electrodes shorted between measurements and by the use of freshly blackened electrodes.

Surface Conductance Measurements. The bulk value of electrolyte conductivity was used in the evaluation of ζ for electrolyte concentrations in excess of 1×10^{-3} mol dm^{-3}. At concentrations $\leq 1 \times 10^{-3}$ mol dm^{-3}, surface conductance measurements were made using the four-electrode method of Schwan.[12] Surface conductivity arises from the establishment of a conduction current by paths other than through bulk liquid. At high electrolyte concentrations, surface conductance was a negligible component of the total conductance.

To measure the conductivity of electrolyte in the streaming potential cell, a dc constant current source capable of supplying between 0.5 and 100 μA was connected to the outer potential measuring electrodes located in the lower Teflon block. The current was measured across a precision resistor using a high input impedance voltmeter. The current was chosen so as not to significantly polarize the electrolyte solutions after current movement for 30 s.[13] A high impedance voltmeter (Analogue Devices 515JH chip) was connected across the inner pair of electrodes and the voltage measured. A frequency of 0.2 Hz was used between measurements in either direction.

A problem common to dc surface conductance measurements is electrode polarization. Extreme cases of electrode polarization have been reported by Van der Linde and Bijsterbosch[14] for porous plug systems with low cell constants. This phenomenon was observed using low surface area "bright" platinum electrodes in contrast to the higher surface area, platinized platinum electrodes used in this study. Tests with reversible Ag/AgCl electrodes confirmed that no significant polarization of the platinum electrodes occurred over the 0.2-Hz time regime.

The conductance of the capillary was calculated using the average current and potentials measured in both directions and the cell constant for the capillary evaluated from the known bulk conductivity and dc conductance at 1×10^{-1} mol dm^{-3} electrolyte concentration. The conductivity of the capillary relative to the measured bulk conductivity was then plotted for each capillary. As noted, capillary conductance measurements were only made for systems in which the electrolyte concentration was $\leq 1 \times 10^{-3}$ mol dm^{-3}.

Cell constants were generally of the order of 120 ± 10 m^{-1} and a typical plot of the conductance of a silica capillary in the presence of KCl at pH 5.8 ± 0.2 is shown in Figure 3. These data show the bulk conductivity requires a correction of $\approx 15\%$ at an electrolyte concentration of 1×10^{-4} mol dm^{-3}. Correction factors obtained by these measurements were used in the calculation of ζ.

Flow Behavior. Flow behavior in a silica capillary was monitored to confirm the fundamental assumption that flow in the capillary was both laminar and established.[15]

The flow rate was measured at applied pressures of $0 \rightarrow 7000$ N m^{-1} ($0 \rightarrow \approx 70$ cm of H_2O) by removing one electrolyte reservoir and at constant pressure, collecting the output of the streaming potential cell in a measuring cylinder for a period of 2 min.

Results for a rectangular capillary of length 7.50 cm and width 2.2 cm are shown in Figure 4. Theoretical results (eq 3) for a plate separation of 0.0120 ± 0.0005 cm are shown for comparison. Allowing for compression of the Teflon gasket in the streaming potential cell, the agreement with predicted flow rates is excellent. Deviations from linearity at low values of ΔP are attributed to an inability to maintain constant pressure at low values (<2000 N m^{-2}) for an extended time interval. The value for η for the viscosity of water at 20 °C was taken from literature sources.[16]

Further to the above flow treatment, Bowen[15] and Van Wagenen and Andrade[8] have suggested the need to have established as well as laminar flow. Fluid flow requires a length to develop an equilibrium flow profile and if this length (Le) is greater than 10% of the total capillary length l, these workers have shown the

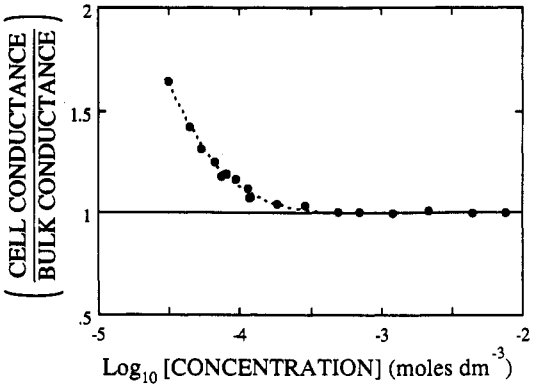

Figure 3. Ratio of the conductivity of a fused silica capillary to the specific conductivity of bulk solution as a function of electrolyte concentration. The electrolyte was KCl and the pH was 5.8 ± 0.2.

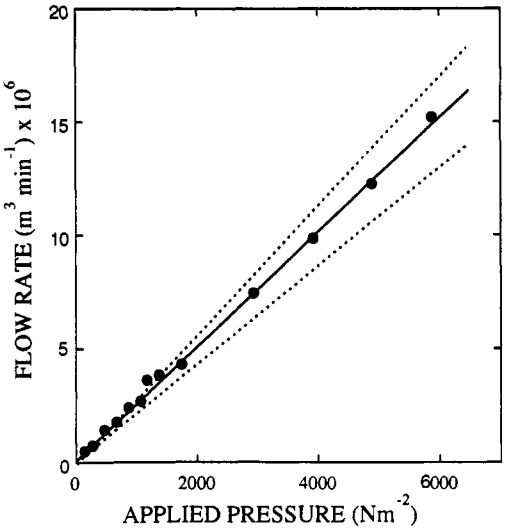

Figure 4. Flow rate of the streaming potential cell versus applied pressure. Dashed lines are theoretical predictions from eq 3 assuming a capillary of width 2.2 cm, length 7.5 cm, and height of 0.0120 ± 0.0005 cm.

measured value of ΔE will be lower than its limiting value. Thus, using the analysis of Bowen, a capillary configuration was chosen with Le $\approx$ 5–6% of l.

Materials. Water used in this study was purified by distillation followed by percolation through charcoal and mixed bed ion exchange resins (Millipore, Milli-Q). The final conductivity of the water was less than 1×10^{-6} S^{-1} cm^{-1} at 20 °C. Experiments were performed at 20 ± 1 °C. Electrolytes were analytical grade reagents. Solvents were analytical or spectroscopy grade.

CIG high purity grade (>99%) nitrogen gas was used for streaming potential measurements and degassing of solutions.

Plates for use in streaming potential measurements were Suprasil grade fused silica and had dimensions of $7.5 \times 2.5 \times 0.1$ cm^3.

Clean, bright platinum electrodes were platinizied using a 3.5% (w/v) solution of chloroplatinic acid doped with 0.005% (w/v) lead acetate by the method of Feltham and Spiro.[17] Electrodes were cleaned in a HCl/HNO_3 mixture followed by rinsing with water and cathodic electrolysis in a 2% (v/v) H_2SO_4 solution for 30 s. The electrodes were then plated in the chloroplatinic acid solution at ≈ 30 mA current for 10 min. Electrodes were uniformly blackened. They were replatinized if this coating deteriorated or if the asymmetry potential in streaming potential measurements increased to a significant level.

Reversible silver/silver chloride electrodes were produced from silver wire by heating to red hot in a gas flame followed by anodic

(12) Schwan, H. P. *Biophysik* **1966**, *3*, 181.
(13) Van Den Hoven, Th. J. J. Ph.D Thesis, Agricultural University, Wageningen, 1984.
(14) Van der Linde, A. H.; Bijsterbosch, B. H. *Colloids and Surf.* **1989**, *41*, 345.
(15) Bowen, B. D. *J. Colloid. Interface Sci.* **1985**, *106*, 367.
(16) *CRC handbook of chemistry and physics*, 60th ed.; Weast, R. C., Ed.; CRC Press: Boca Raton, FL, 1981.
(17) Feltham, A. M.; Spiro, M. *Chem. Rev.* **1971**, *71*, 177.

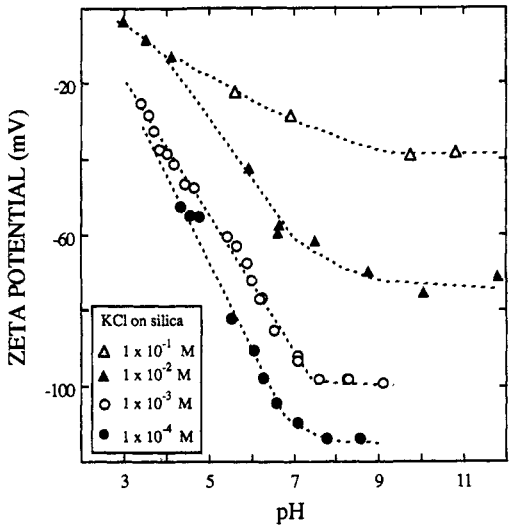

Figure 5. Zeta potential of a fused silica capillary versus pH in aqueous solutions of KCl.

deposition of a silver chloride coating in a concentrated chloride solution.[18]

General laboratory glassware was cleaned by soaking in a hot alkaline detergent (Extran) solution followed by immersion in strong alkali and warm concentrated nitric acid and thorough rinsing with water. It was then dried in an oven at 100 °C.

Fused silica plates were polished with a fine (<50 nm) polishing slurry for 10 min, soaked in hot alkaline detergent, rinsed with water, and cleaned in an ammonical peroxide solution as per the method of Lamb and Furlong.[19] The plates were then rinsed with water and dried in an oven at 100 °C.

Results

A plot of the zeta potential of a fused silica capillary as a function of pH in aqueous solutions of KCl is shown in Figure 5. Potentials were calculated using the Smoluchowski equation and corrected for surface conductance effects using the data of Figure 3. Extrapolated data show the silica to have an isoelectric point of 2.8 ± 0.2 pH units. This is slightly higher than the values reported by Wiese et al.[1] for fused silica and Bousse et al.[9] for thin film silica but well within the limits of other studies reported by Parks.[20] The magnitude of the maximum zeta potential reported at each electrolyte concentration is within ±5 mV of the studies of Wiese et al. and Li and DeBruyn[4] and if one considers the difference between the silica and the capillary apparatus used for each study, the agreement is excellent. The error on each data point is estimated at ±2 mV for electrolyte concentrations $\leq 1 \times 10^{-2}$ mol dm^{-3} and at ±4 mV for greater concentrations. The error enhancement at higher added electrolyte is due to the decreased precision in the voltage measurement under these solution conditions.

Model Considerations. The most widely encountered model of the electrical double layer (edl) using a Poisson–Boltzmann distribution of ions in the diffuse double layer and a GCSG type approach to the inner double layer region is the triple layer model proposed by Yates et al.[21] This model assumes the edl to be divided into a diffuse and bound region, the latter of which is further divided into an inner and outer capacitive layer having dielectric constants of D_1 and D_2 and capacitances of C_1 and C_2, respectively. The point of closest approach of hydrated double layer ions is then the edge of the outer layer at a distance d from the surface (commonly referred to as the outer Helmholtz plant [OHP]) and to a distance β, the edge of the inner region (commonly referred to as the inner Helmholtz plane [IHP]) for bound ionic species. This double layer model has an electroneutrality condition of the form

$$\sigma_o + \sigma_\beta + \sigma_d = 0 \tag{4}$$

where σ_o, σ_β, and σ_d are the surface charge at the surface, IHP, and OHP, respectively.

We can now write down the dissociation equilibria and equilibrium constants for an oxide surface site, S

$$SH_2^+ \leftrightarrow SH + H_s^+ \qquad (K_+)$$

$$SH \leftrightarrow S^- + H_s^+ \qquad (K_-)$$

$$SH_2A \leftrightarrow SH + H_s^+ + A_s^- \qquad (^*K_A)$$

$$SH + M_s \leftrightarrow SM + H_s^+ \qquad (^*K_M)$$

where the s subscript refers to a surface as distinct from a bulk species and the M and A subscripts represent cationic and anionic electrolyte species, respectively.

Typically, a surface binding constant has the form

$$^*K_M = \left(\frac{[SM]\, a(H^+)_s}{[SH]\, a(M^+)_s}\right) \tag{5}$$

where $a(H^+)_s$ and $a(M^+)_s$ are the activity of the hydrogen and metal ions at the surface, respectively. Assuming a Poisson–Boltzmann distribution of ions, the activity of surface species may be related to the activity of similar species in the bulk by

$$a_s(H^+) = a_b(H^+) \exp\left(-\frac{e\psi_0}{kT}\right) \tag{6}$$

In this equation, $a_b(H^+)$ is the proton activity in the bulk and ψ_0 is the electrostatic surface potential. For the case of a metal ion at the surface, this becomes

$$a_s(M^+) = a_b(M^+) \exp\left(-\frac{e\psi_\beta}{kT}\right) \tag{7}$$

where ψ_β is the potential of the plane of closest approach of a counterion to the surface using the analogy of Davis et al.[22] and $a_b(M^+)$ is the bulk electrolyte activity.

The surface charge per unit area is then given by

$$\sigma_o = e([SH_2^+] + [SH_2A] - [S^-] - [SM]) \tag{8}$$

the charge at the IHP as

$$\sigma_\beta = e([SM] - [SH_2]) \tag{9}$$

and the total number of surface sites per unit area as

$$N_s = [SH_2^+] + [SH_2A] + [SH] + [S^-] + [SM] \tag{10}$$

where the surface concentrations are in terms of sites per unit area. Using the electroneutrality relationship of eq 4 and the Gouy–Chapman relationship between charge and potential for symmetrical electrolytes[23] yields

(18) Bates, R. G. *Determination of pH, theory and practice*; Wiley: New York, 1973; p 328.
(19) Lamb, R. N.; Furlong, D. N. *J. Chem. Soc., Faraday Trans. 1* **1982**, *78*, 61.
(20) Parks, G. A. *Chem. Rev.* **1964**, *65*, 177.
(21) Yates, D. E.; Levine, S.; Healy, T. W. *J. Chem. Soc., Faraday Trans.* **1974**, *70*, 1807.
(22) Davis, J. A.; James, R. O.; Leckie, J. O. *J. Colloid. Interface Sci.* **1978**, *63*, 480.
(23) Reference 10, p 29.

$$\sigma_d = e([S^-] - [SH_2^+]) = \left(\frac{-2\kappa D\epsilon_o kT}{e}\right) \sin\left(\frac{e\psi_d}{2kT}\right) \quad (11)$$

where κ is the inverse Debye length. If ions are bound such that any micropotential terms[24] can be neglected or are constant, and assuming activities may be reasonably approximated by concentrations for dilute electrolyte systems, then eq 5 may be rewritten in the form

$$^*K_M = \left(\frac{[SM][H^+]_s}{[SH][M^+]_b}\right) \exp\left(\frac{e\psi_\beta - e\psi_0}{kT}\right) \quad (12)$$

By rearrangement of the above system of equations, the surface concentrations of $[SH_2A]$, $[SH_2^+]$, [SM], [SH], and $[S^-]$ may be found. Typically, the pK values for the ionization equilibria then take the form

$$pK_+ = pH + \log_{10}[SH_2^+] - \log_{10}[SH] + \left(\frac{e\psi_0}{2.303kT}\right) \quad (13)$$

and

$$pK_- = pH - \log_{10}[S^-] + \log_{10}[SH] + \left(\frac{e\psi_0}{2.303kT}\right) \quad (14)$$

Using these equations and those given by Yates et al.[21] which relate the potential at the surface to the surface charge density, the charge–potential relationship across the interface as a function of pH and electrolyte concentration may be computed.

Before the analysis can proceed, the site dissociation constants, K_+ and K_-, ion binding constants, $^*K_A$ and $^*K_M$, and the inner and outer layer capacitances, C_1 and C_2, all need to be assigned appropriate values.

Generally, the K_+ and K_- ionization constants are obtained from the double extrapolation technique of charge versus pH data proposed by James and co-workers.[22,25,26] Values for $^*K_A$ and $^*K_M$ are obtained by a similar but not identical technique. Alternatively, the surface ionization constants, K_+ and K_-, may be estimated from electrokinetic data using the procedure of Sprycha and Szczypa.[27] Other values must be taken from literature sources.

To evaluate the surface ionization constants, Sprycha and Szczypa first make the approximation that for pH $\gg$ pH_{pzc} (where pH_{pzc} is the pH of the point of zero charge of the surface) eq 8 is approximated by[28]

$$\sigma_o \approx -e([S^-] + [SM]) \quad (15)$$

and for pH $\ll$ pH_{pzc}

$$\sigma_o \approx +e([SH_2^+] + [SH_2A]) \quad (16)$$

Using the assumption $\psi_d \approx \zeta$ for low ionic strengths (<0.01 mol dm^{-3}) and $\sigma_\beta = 0$ at the pzc (no specific adsorption), then σ_d is approximately given by

$$\sigma_d \approx e([S^-]) \text{ for pH} \gg pH_{pzc} \quad (17)$$

The approximations for pH $\ll$ pH_{pzc} are ignored from this point of the discussion since they have little relevance for a silica interface. The value of $[S^-]$ is now in terms of known quantities and with the further assumption of

$$N_s \approx [SH] \quad (18)$$

the pK values may be evaluated. Smith[29] has shown that eq 19 is a reasonable assumption for oxide systems at *low electrolyte concentration.*

A value for N_s was chosen based on consideration of the nature of the fused silica surface and on a literature perusal of the various determinations that have been made on such a surface. The surface of crystalline silica is known to consist of both silanol groups and siloxane bridges, siloxane bridges being formed through the mutual condensation of silanol groups. The presence of silanol groups is presumed to dominate at low temperature with condensation to siloxane occurring at ≈850 °C. The wettability and reactivity of the solid decrease accordingly and have been thoroughly investigated.[19,30]

The density of these silanol sites on silica is generally found to be ≈20 Å^2 site^{-1} [31] or 5×10^{14} sites cm^{-2}. The exact number density of ionizable sites, which is important to the theoretical modeling of the surface, varies with silica type and its history. The maximum number of *reactive surface sites*[32] can be measured by use of a tritium exchange procedure. Yates et al.[33,34] examined a number of oxide systems and found that an ionizable site density value of 20 Å^2 site^{-1} was a poor estimate for a number of silica types. They tested two samples with similar properties to fused silica and found a silanol site area of (3.8 and 2.4) $\times 10^{14}$ sites cm^{-2}. Their average value of 3.1×10^{14} sites cm^{-2} (≈32 Å^2 site^{-1}) is probably a better value to assume in calculations involving the fused silica surface. It is our opinion that the maximum charge density estimated from tritium exchange work is more representative of the number of sites available for ionization on the silica examined in this study and is more typical of titration values obtained on nonporous calcined silica.[35–37]

We can proceed by introducing the acidity quotient pQ_-[22] such that

$$pQ_- = pK_- - \left(\frac{e\psi_0}{2.303kT}\right) = pH - \log_{10}[S^-] + \log_{10}[SH] \quad (19)$$

In terms of the former approximations

$$pQ_- = pH + \log_{10}[N_s] - \log_{10}\left[\left(\frac{-2\kappa D\epsilon_o kt}{e^2}\right) \sinh\left(\frac{e\zeta}{2kT}\right)\right] \quad (20)$$

Plots of pQ_- versus pH interpolated to pH_{iep} for electrokinetic data (ie. $\psi_0 \rightarrow 0$) should give a unique pK for the oxide system. James and Parks use a similar procedure for interferring the binding constants, $^*K_A$ and $^*K_M$, from potentiometric titration data. In a later paper, Sprycha and Szczypa[38] showed that the slope of a pQ versus pH plot should be representative of the change in the surface potential (ψ_0) as a function of pH. This slope is calculated

(24) Levine, S.; Smith, A. L. *J. Chem. Soc., Faraday Discuss.* **1971**, *52*, 290.
(25) James, R. O.; Parks, G. A. In *Surface and colloid science*; Matijevic, E., Ed.; Plenum: New York, London, 1982; Vol. 7, p 119.
(26) James, R. O. *Adv. Ceram.* **1987**, *21*, 349.
(27) Sprycha, R.; Szczypa, J. *J. Colloid. Interface Sci.* **1984**, *102*, 288.
(28) Davis, J. A.; Leckie, J. O. *J. Colloid. Interface Sci.* **1978**, *67*, 90.
(29) Smith, A. L. *J. Colloid. Interface Sci.* **1976**, *55*, 525.
(30) Hair, M. L. *Infrared spectroscopy in surface chemistry*; Marcel Dekker, Inc.: New York, 1967.
(31) Van der Voort, P.; Gillis-D'Hamers, I.; Vansant, E. F. *J. Chem. Soc., Faraday Trans.* **1990**, *86*, 3751.
(32) Bérubé, Y. G.; Onoda, G. Y.; deBruyn, P. L. *Surf. Sci.* **1967**, *8*, 449.
(33) Yates, D. E.; Healy, T. W. *J. Colloid. Interface Sci.* **1976**, *55*, 9.
(34) Yates, D. E.; Grieser, F.; Cooper, R.; Healy, T. W. *Aust. J. Chem.* **1977**, *30*, 1655.
(35) Abendroth, R. P. *J. Phys. Chem.* **1957**, *76*, 2547.
(36) Bolt, G. H. *J. Phys. Chem.* **1957**, *61*, 1166.
(37) Yates, D. E., Ph.D Thesis, University of Melbourne, 1975.
(38) Sprycha, R.; Szczypa, J. *J. Colloid. Interface Sci.* **1987**, *115*, 590.

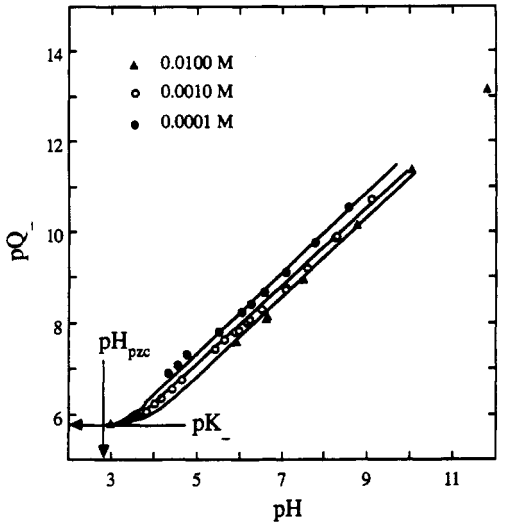

Figure 6. Acidity quotient (pQ_-) for a fused silica capillary versus pH in aqueous solutions of KCl. Interpolation to the iep gives a pK_- value of 5.8.

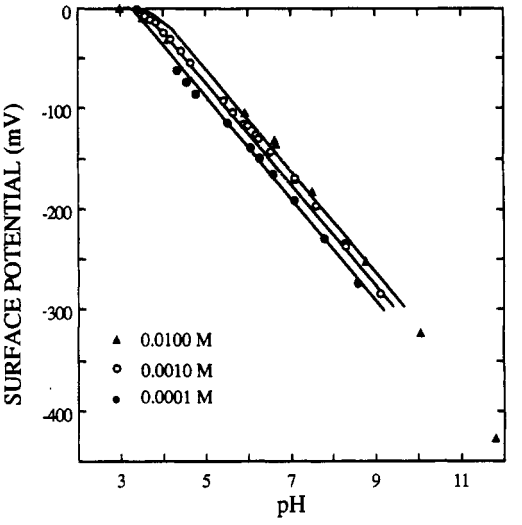

Figure 7. Calculated surface potential for a fused silica capillary versus pH in aqueous solutions of KCl. Data were calculated assuming a pK_- value of 5.8.

using the model of Davis et al.,[22] which generalizes eq 19, to give

$$pK - pQ = \left(\frac{-e\psi_0}{2.303kT}\right)$$

and then

$$-\left(\frac{d(pQ)}{d(pH)}\right) = \frac{d}{d(pH)}\left(\frac{e\psi_0}{2.303kT}\right) \quad (21)$$

Deviation from linearity is expected at pH values close to the iep due to the breakdown in the assumption of eq 17 and at high degrees of ionization due to the breakdown of the assumption, $N_s \approx$ [SH]. Following the above analysis, a plot of pQ_- versus pH for the fused silica capillary in aqueous solutions of KCl at concentrations from 1×10^{-2} to 1×10^{-4} mol dm^{-3} is shown in Figure 6. Using the curve–linear interpolation method of Sprycha and Szczypa,[38] the data are interpolated to the iep to give a pK_- value for fused silica of 5.8. The slope of the line (pQ_- versus pH) for pH $\gg$ pH_{pzc} gives an average slope in ψ_0 of 54 ± 2 mV per pH unit (ΔpH $\gg$ 4). This is ≈5 mV per pH unit less than the Nernstian slope at 20 °C and is in close agreement with the slope predicted using the data of Wiese et al.[1] for a value of pK_- of 5.8 and using eq 21. A plot of pH versus ψ_0 is shown in Figure 7.

For a truly amphoteric surface site, a relationship between pK_+, pK_-, and pH_{pzc} can be introduced, such that

$$pH_{pzc} = \left(\frac{pK_- + pK_+}{2}\right) \quad (22)$$

and

$$\Delta pK_\pm = pK_- - pK_+ \quad (23)$$

From the pK data obtained in Figure 6 and eqs 22 and 23, values of pK_+ = −0.2 and $\Delta pK_\pm$ = 6.0 are calculated for fused silica.

$\Delta pK_\pm$ is an interesting quantity and is most easily envisaged as a measure of the relative strengths of the two surface acids, SH and SH_2^+.[39] Levine and Smith[24] show that for large values of $\Delta pK_\pm$ (i.e. $\Delta pK_\pm \rightarrow 10$), the fraction of negative and positives sites to total sites at the pzc tends to zero, or alternatively, [SH] → N_s. In contrast to this, for a Nernstian surface, the fraction of negative sites to total sites approaches 0.5 as $\Delta pK_\pm \rightarrow -\infty$. The rigour of our method is seen to be greatest for the former case.

The calculated value of $\Delta pK_\pm$ is in good agreement with other studies of crystalline silica systems.[27,40] The $\Delta pK_\pm$ value of 6.0 calculated for silica also lends weight to the assumption of [SH] ≈ N_s used in the calculation of pK_-. In so doing, it validates the model of Sprycha and Szczypa[27] for pH $\gg$ pH_{pzc}. However, although this procedure appears reasonable for $\Delta pK_\pm$ values of 6, the validity of the assumption across a range of pH values must be questioned for lower values of $\Delta pK_\pm$ and particularly at significantly smaller values of N_s.

Reasonable values for the inner and outer layer capacitances and values for the ion binding constants $*K_M$ and $*K_A$ are now required. Milonjic[41] reports p$*K_M$ values for Li^+, Na^+, K^+, and Cs^+ ions on a colloidal amorphous silica obtained by the double extrapolation method of Davis et al.[22] Values of pK_- = 8.2 and p$*K_M$(KCl) = 7.0 were obtained. This represents a specific adsorption energy of +15.7 kJ mol^{-1} at 25 °C as calculated using the chemical adsorption potential described by Yates et al.[21] and a free energy of adsorption of 38.7 kJ mol^{-1} as calculated using

$$\Delta G = -kT \ln (*K_M) \quad (24)$$

Dugger et al.[40] also obtained a free energy of adsorption value close to that of Milonjic[41] for a silica gel/KNO_3 system at 20 °C. Other workers[22,42] report a value of 38.2 kJ mol^{-1} for a pyrogenic silica/KCl system at 25 °C. No literature values are apparent for more crystalline samples since the specific surface area of such samples is generally quite low and analysis of titration data is correspondingly difficult. Although the surface site acidity is expected to change with increasing surface structure, the adsorption of metal ions should remain moderately constant.

Therefore, a starting value of p$*K_M$ of 6.8 was chosen (assuming an equivalent ΔG to Milonjic) for model calculations although a slightly lower value may be appropriate in light of the shift of pK_- value associated with the increased surface structure of the fused silica used here. This shift is exemplified by a value of pK_- of 5.3 calculated for an α-quartz system by Dugger et al.[40] As expected, the value is substantially lower than the pK_-

(39) Healy, T. W.; White, L. R. *Adv. Colloid. Interface Sci.* **1978**, *9*, 303.

(40) Dugger, D. L.; Stanton, J. H.; Irby, B. N.; McConnell, B. L.; Cummings, W. W.; Maatman, R. W. *J. Phys. Chem.* **1964**, *68*, 157.

(41) Milonjic, S. K. *Colloids Surf.* **1987**, *23*, 30.

(42) Reference 24, p 185.

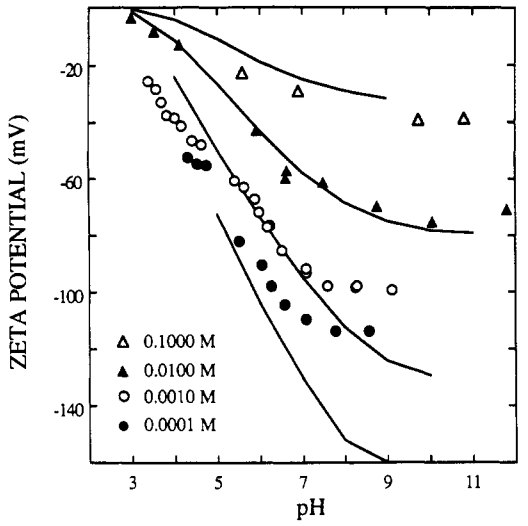

Figure 8. Zeta potential of a fused silica capillary as predicted by the GCSG model. Solid lines are theory; points are experimental. Modeling parameters used were $\Delta pK_{\pm} = 6.0$, $pH_{iep} = 2.8$, $\Delta p^*K_{AM} = 8.0$, $C_1 = 140\ \mu F\ cm^{-2}$, and $C_2 = 20\ \mu F\ cm^{-2}$.

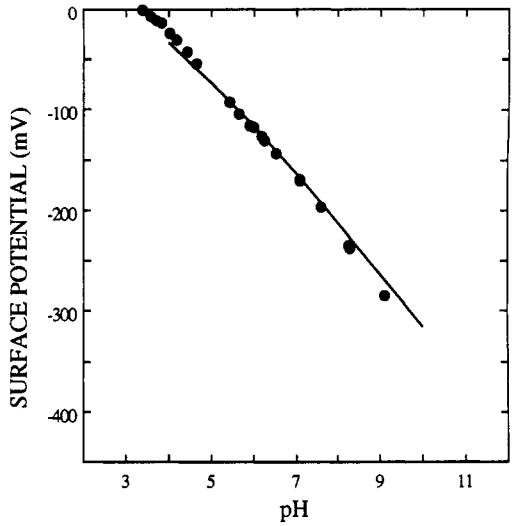

Figure 9. Comparison of the surface potential calculated from the GCSG model with experimentally predicted potentials. All model parameters are as for Figure 8. Electrolyte concentration was 0.001 mol dm^{-3}.

value calculated for amorphous silica samples.[41] The value of $pK_- = 5.8$ interpolated from Figure 6 is consistent with the above line of argument. Errors in pK_- are principally associated with the value of N_s (the total number of surface sites per unit area). Although a significant miscalculation of this value is possible, pK_- would only vary by ±0.2 pK unit for a variation in N_s from (2 to 5) × 10^{14} sites cm^{-2}.

Literature values for the inner and outer layer capacitances vary greatly. The exact values are likely to remain a case in point since integral capacitances are not available for the silica aqueous interface. This is not so for the Hg and Ag halide based systems which may be fabricated into conducting electrodes. From potentiometric titration data, Yates et al.[21] and Healy and White[39] calculated a value of C_1 of 100–140 $\mu F\ cm^{-2}$. A similar value has been obtained[43] (i.e. 150 $\mu F\ cm^{-2}$) from the slopes of pQ_M versus degree of ionization plots. Values for C_2 are generally assumed to be lower than C_1 and of the order of 20 $\mu F\ cm^{-2}$.[21,25,43] Studies on α-Al_2O_3 single crystals[44] suggest values of <10 $\mu F\ cm^{-2}$ and possibly values as low as 4–6 $\mu F\ cm^{-2}$. This latter study used a modified site binding model in which the diffuse layer potential was weighted over contributions from both free (S^-) and complexed (SM) sites. The value for C_2 of 20 $\mu F\ cm^{-2}$ has gained some consensus of use and was therefore used on our silica data.

Model Predictions. The theoretical predictions of the site binding model for the values $pK_+ = -0.2$, $pK_- = 5.8$, $pH_{pzc} = 2.8$, $p^*K_A = -1.2$, $p^*K_M = 6.8$, $C_1 = 140\ \mu F\ cm^{-2}$, and $C_2 = 20\ \mu F\ cm^{-2}$ are shown in Figure 8 for pH versus the OHP potential, $\psi_d = \zeta$.

Although results for the calculated potential versus pH data are overall in excellent agreement with the experimental results at 1×10^{-2} mol dm^{-3}, the calculations tend to overestimate the potential at lower electrolyte concentrations and underestimate the potential at higher concentrations. Calculated surface charge versus pH data are in reasonable agreement with observed potentiometric titration data.[35-37,41]

The trends observed in the model calculations are typical of those found from similar analyses of TiO_2 and Al_2O_3 systems.[21,28,39,45] The surface potential versus pH data from experimental and model calculations are shown in Figure 9. Only the 1×10^{-3} mol dm^{-3} data are shown for clarity. A good fit to the data is obtained at a ΔpH_{iep} of between 1 and 5 (i.e. pH 3.8–8.8) but deviations occur close to the iep and at higher ionization. This is possibly due to a breakdown in the assumptions of $-\sigma_d \approx [S^-]$ and $[SH] \approx N_s$, respectively. This possibility may be tested by taking the pH versus ψ_d data generated by the model, analyzing the data using the method of Sprycha and Szczypa,[27] and comparing the resultant pH versus ψ_0 data. The differences are highlighted in a plot of the slope of the surface potential as function of pH versus ΔpH as shown in Figure 10.

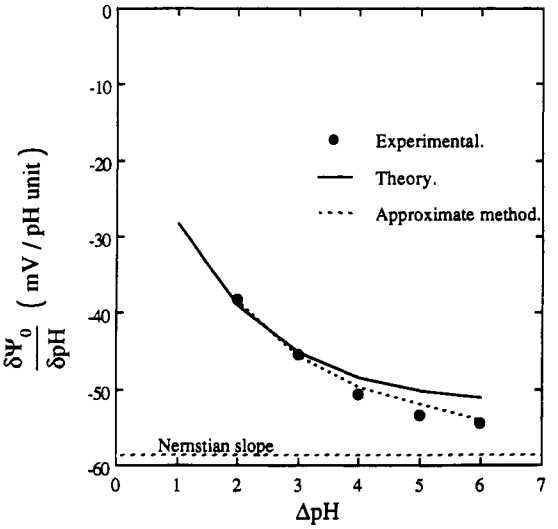

Figure 10. Slope of the surface potential for a fused silica capillary versus the difference in pH units from the iep. Electrolyte concentration was 0.01 mol dm^{-3} KCl. Solid line was calculated using the model parameters of Figure 8; dashed line was calculated using the theory of Sprycha and Szczypa.[25]

The plot clearly shows the breakdown in the approximate technique for $\Delta pH > 4$ (i.e. pH > 6.8). Data were generated by taking the slope of a fifth-order polynomial fit to the ψ_0 versus ΔpH data. Allowing for the breakdown in the analysis at high ΔpH, this exemplifies the excellent fit to data produced by the GCSG model for these

(43) Blesa, M. A.; Figliolia, N. M.; Moroto, A. J. G.; Regazzoni, A. E. *J. Colloid Interface Sci.* **1984**, *101*, 410.
(44) Smit, W. *J. Colloid. Interface Sci.* **1986**, *109*, 295.
(45) Westall, J.; Hohl, H. *Adv. Colloid. Interface Sci.* **1980**, *12*, 265.

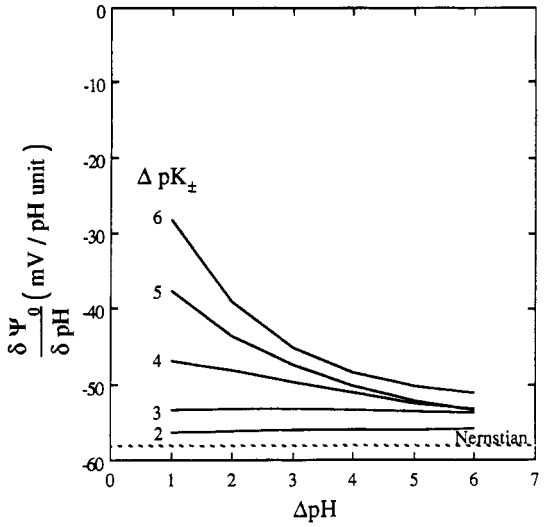

Figure 11. Slope of the surface potential versus difference in pH units from the pzc. Electrolyte concentration was 0.01 mol dm^{-3}. Lines are for various values of $\Delta pK_{\pm}$.

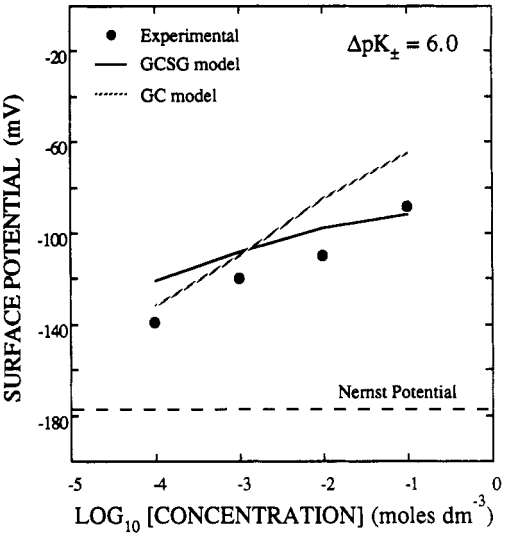

Figure 12. Comparison of the slope of the surface potential versus electrolyte concentration for the GCSG model, the GC model, and experiment at pH 5.8.

experimental data. The fit of the model to the slope of the surface potential, the zeta potential, and the charge, as a function of pH, is indeed a stringent test, even if only at a single electrolyte concentration.

The dependence of ψ_0 on ΔpH, concentration and $\Delta pK_{\pm}$ was predicted by Healy et al.[46] in 1977 for a 1×10^{-2} mol dm^{-3} aqueous 1:1 electrolyte system and again by Healy and White[39] for a 1×10^{-3} mol dm^{-3} system. At constant electrolyte concentration, the dependence of the slope in ψ_0 with pH as a function of the value of $\Delta pK_{\pm}$ was predicted to be quite significant. Indeed, for a $\Delta pK_{\pm} = 6$ system, the maximum slope in ψ_0 per pH unit was calculated analytically to be 39.7 mV at a ΔpH value of 3–4. This is quite different from the maximum of 51 ± 1 mV per pH unit predicted by the GCSG model and the maximum of ≈ 54 ± 3 mV per pH unit calculated from experimental data.

The discrepancy between the slopes of $(d\psi_0/dpH)$ calculated in this study and those calculated by Healy and co-workers[39,46] is associated with the difference in the basic models used in the data analysis. The GCSG model quite obviously provides an improved description of the electrical double layer for the fused silica case. An analysis of the $(d\psi_0/dpH)$ versus ΔpH for $\Delta pK_{\pm}$ values between 2 and 6, as calculated using the GCSG model, is shown in Figure 11. Input parameters were $\Delta pK_{AM} = 8.0$, $C_1 = 140$ μF cm^{-2}, $C_2 = 20$ μF cm^{-2}, and $N_s = 3.1 \times 10^{14}$ sites cm^{-2}. Even though the present analyses is possibly as incomplete as that of Healy and co-workers in providing a complete description of the edl, the changes in $(d\psi_0/dpH)$ as the value of $\Delta pK_{\pm}$ decreases from 6 to 2 are far less marked than in the original description. As before, the slope moves toward the Nernstian value as $\Delta pK_{\pm}$ decreases but the sharp decrease in slope as ΔpH increases is not as pronounced. The decrease in slope becomes more obvious if N_s is also decreased.

The prediction of the dependence of ψ_0 on electrolyte concentration is also different between the GCSG and the Gouy–Chapman model. Sprycha and Szczypa[27] have observed a strong concentration dependence of ψ_0 for both an Al_2O_3/KNO_3[47] and a TiO_2/KNO_3[48] system. This is in line with eqs 19 and 20 where a κ dependence is predicted.

A similar dependence is observed in Figure 6. As with the previous discussion, the GCSG model predicts a less pronounced dependence of ψ_0 on electrolyte concentration than the Gouy–Chapman model. A comparison of the dependence between the GCSG model, the Gouy–Chapman model, and the experimentally predicted values at $\Delta pK_{\pm} = 6$ and at ΔpH = 3 is shown in Figure 12. The fit by either model is not exceptional, although deviation of the GCSG model is less marked.

The next step in the analysis of the GCSG model is to look at the changes required to produce a fit to the data in Figure 5. This requires an adjustment of the site binding constants. As noted, the model tends to overestimate the zeta potential at low electrolyte concentration and underestimate the potential at high electrolyte concentration.

Given that the fit to the charge data is good, no adjustment of the inner layer capacitance, C_1, seems appropriate. For the potential data, an adjustment in the outer plane capacitance, C_2, is required to give a better approximation to the calculated zeta potential. This is equivalent to shifting the position of the shear plane or, alternatively, inducing an apparent change in the dielectric of the outer layer. To gain some appreciation of the change required in C_2 to obtain a reasonable convergence between theory and experiment, C_2 needs to be varied from a value of 30 μF cm^{-2} at 1×10^{-1} mol dm^{-3} to 4 μF cm^{-2} at 1×10^{-4}. The results of this fitting exercise are shown in Figure 13. The fit to the data at low electrolyte concentration is still not perfect although much improved over the constant capacitance condition.

Since by definition

$$C_2 = D\epsilon_0/d \tag{25}$$

where d is the distance between the IHP and OHP, a change in C_2 from 4 to 30 μF cm^{-2} is the equivalent of a proportional inward shift in the arbitrary plane of shear or a proportional increase in the dielectric constant of the medium in the compact layer. No evidence exists to justify either of these hypotheses and, therefore, it remains to be said that the site binding model does not fully describe the charge–potential profile for the silica interface. The model used does however give a better understanding and fit to data than many of the earlier and less elaborate models to describe the potential profile for oxide systems.

(46) Healy, T. W.; Yates, D. E.; White, L. R.; Chan, D. Y. *J. Electroanal. Chem. Interfacial Electrochem.* **1977**, *80*, 57.
(47) Smit, W.; Holten, C. L. M. *J. Colloid. Interface Sci.* **1980**, *78*, 1.
(48) Wiese, G. R.; Healy, T. W. *J. Colloid. Interface Sci.* **1975**, *51*, 427.

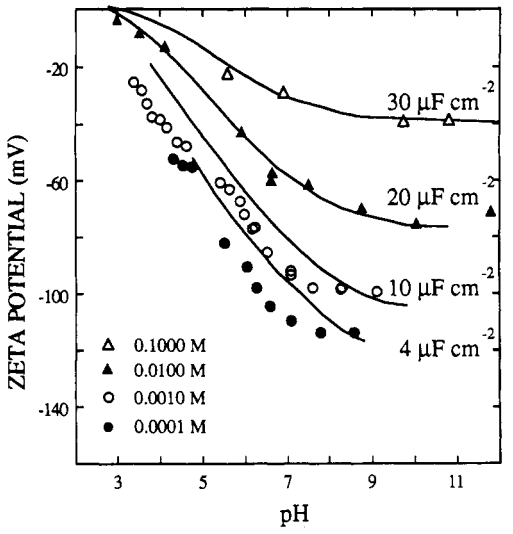

Figure 13. GCSG model of the silica–solution interface with a variable outer layer capacitance (C_2). All other model parameters are as for Figure 8.

Conclusions

The site binding model of the silica–solution interface gives an adequate but not perfect description of the experimental zeta potential data. This description was in terms of calculated and deduced model parameters. An adjustable outer layer capacitance was required in all cases.

The analysis of the zeta potential data using the method of Sprycha and Szczypa[27] was found to be useful in examining the trends in both the surface potential and the slope of the surface potential as a function of pH. Use of the site binding model to examine the range of effectiveness of the surface potential approximation also gives interesting information on the slope of the surface potential as a function of both ΔpH and $\Delta pK_{\pm}$.

Acknowledgment. This work was supported by an Australian Research Council program grant.

Appendix

The development of flow equations for a rectangular capillary of width w, length l, and height h is achieved by first considering the equation of motion for an incompressible fluid in a gravitational field g[2]

$$\rho_f(\mathbf{v}\cdot\nabla)\mathbf{v} = \rho_f\left(\frac{\partial\bar{\mathbf{v}}}{\partial t}\right) = \rho_f g - \nabla P + \eta\nabla^2\mathbf{v} \qquad \text{(A1)}$$

In this equation, ρ_f is the density of the fluid and $\mathbf{v}$ is the fluid velocity. At low fluid velocities the inertial term, ρ_f $(\mathbf{v}\cdot\nabla)$ $\mathbf{v}$ is small. Under steady-state conditions (i.e. the rate of change of velocity with time = 0) and with the neglect of gravitational effects due to the small dimensions of the capillary, eq A1 reduces to

$$\eta\nabla^2\mathbf{v} - \nabla\rho = 0 \qquad \text{(A2)}$$

With laminar flow under an applied pressure gradient in the y direction we have

$$\nabla\cdot\mathbf{v} = 0 \qquad \text{(A3)}$$

and

$$\mathbf{v} = v(x,z)\hat{y} \qquad \text{(A4)}$$

Equation A2 then reduces to

$$\eta\left(\frac{\partial^2 v}{\partial z^2} + \frac{\partial^2 v}{\partial x^2}\right) - \frac{\partial P}{\partial y} = 0 \qquad \text{(A5)}$$

and

$$\frac{\partial P}{\partial x} = \frac{\partial P}{\partial y} = 0$$

Taking the partial derivative of eq A5 with respect to y gives

$$d^2P/dy^2 = 0 \qquad \text{(A6)}$$

since v is independent of y. This may be integrated to give

$$P = P_0 - \left(\frac{\Delta P}{l}\right)y$$

where P_0 is the pressure at $y = 0$ and ΔP is the pressure difference between the two ends of the channel. The pressure gradient is given by

$$\frac{dP}{dy} = -\left(\frac{\Delta P}{l}\right) \qquad \text{(A7)}$$

We first consider the simpler case of a narrow capillary $h \ll w$, where we can ignore x derivatives relative to z derivatives (i.e. assuming the effects of the capillary side walls are small), then eq A5 becomes

$$\eta\left(\frac{d^2 v}{dz^2}\right) + \left(\frac{\Delta P}{l}\right) = 0 \qquad \text{(A8)}$$

For Poiseuille flow, we have $v = 0$ at both $z = 0$ and $z = h$ and, hence, the fluid velocity is

$$v = \left(\frac{z(h-z)}{2\eta}\right)\left(\frac{\Delta P}{l}\right) \qquad \text{(A9)}$$

This expression describes the average fluid velocity in the capillary ignoring side wall effects. The flow rate Q is now calculated as

$$\begin{aligned} Q &= w\int_0^h v\,dz \\ &= w\int_0^h\left[\left(\frac{z(h-z)}{2\eta}\right)\left(\frac{\Delta P}{l}\right)\right]dz \\ &= \left(\frac{wh^3\Delta P}{12\eta l}\right) \end{aligned} \qquad \text{(A10)}$$

For the general case of arbitrary capillary aspect ratios, we seek a solution of eq A5 of the form

$$v(x,z) = \left(\frac{z(h-z)}{2\eta}\right)\left(\frac{\Delta P}{l}\right) + \omega(x,z) \qquad \text{(A11)}$$

where

$$\left(\frac{\partial^2\omega}{\partial x^2}\right) + \left(\frac{\partial^2\omega}{\partial z^2}\right) = 0 \qquad \text{(A12)}$$

with the boundary conditions

$$\omega(x,0) = \omega(x,h) = 0 \qquad \text{(A13a)}$$

and

$$\omega(0,z) = \omega(w,z) = \left[\left(\frac{-z(h-z)}{2\eta}\right)\left(\frac{\Delta P}{l}\right)\right] \qquad \text{(A13b)}$$

which ensures that the fluid velocity vanishes at the capillary walls. Putting $\omega = (x,z) = X(x)Z(z)$, eq A12 becomes

$$\left(\frac{X''}{X}\right) = \left(\frac{-Z''}{Z}\right) = \text{constant} = -p^2 \qquad \text{(A14)}$$

The solution for $Z(z)$ that satisfies [A13a] is

$$Z(z) = \sin(pz) \tag{A15}$$

with

$$p = (n\pi/h) \qquad n = 1, 2, \ldots$$

and a solution for $X(x)$ that is symmetrical about $x = (w/2)$ is

$$X(x) = \cosh\left[\left(\frac{n\pi}{h}\right)\left(x - \left(\frac{w}{2}\right)\right)\right] \tag{A16}$$

Thus the general solution of eq A12 that satisfies [A13a] is

$$\omega(x,z) = \sum_{n=1}^{\infty} A_n \cosh\left[\frac{n\pi}{h}\left(x - \left(\frac{w}{2}\right)\right)\right] \sin\left[\frac{n\pi z}{h}\right] \tag{A17}$$

where the coefficients A_n must now be chosen to satisfy eq A13b. On the interval $0 \le z \le h$, $z(h - z)$ can be represented by the Fourier sine series

$$z(h-z) = \frac{8h^2}{\pi^3} \sum_{m=0}^{\infty} \frac{1}{(2m+1)^3} \sin\left(\frac{(2m+1)\pi z}{h}\right) \tag{A18}$$

Combining this result with eqs A11, A13b, and A17, we obtain the final expression for the velocity

$$v(x,z) = \frac{z(h-z)\Delta P}{2\eta l} - \left(\frac{4h^2\Delta P}{\pi^3 \eta l}\right) \times \sum_{m=0}^{\infty} \frac{\cosh\left[\left(\frac{(2m+1)\pi}{h}\right)\left(x - \frac{w}{2}\right)\right] \sin\left[\frac{(2m+1)\pi z}{h}\right]}{(2m+1)^3 \cosh\left[\frac{(2m+1)\pi w}{2h}\right]} \tag{A19}$$

The flow rate, Q, is given by

$$Q = \int_0^w dx \int_0^h dz\, v(x,z)$$

$$= \frac{wh^3\Delta P}{12\eta l} - \left(\frac{16h^4\Delta P}{\pi^5 \eta l}\right) \sum_{m=1}^{\infty} \frac{1}{(2m+1)^5} \tanh\left(\frac{(2m+1)\pi w}{2h}\right) \tag{A20}$$

Registry No. SiO_2, 60676-86-0; KCl, 7447-40-7.